ERRATA

THIRD INTERIM ENGINEERING REPORT
CONTRACT AF-33(657)-8995

The theoretical R_{eq} curve originally shown in Figure 9 was plotted from computer data which, because of the input parameters used, were not appropriate to the experimental tubes discussed in the report. The attached graph presents the results of a computation of R_{eq} for values of Z_c, Cd, Q, and N, which more accurately describes these tubes.

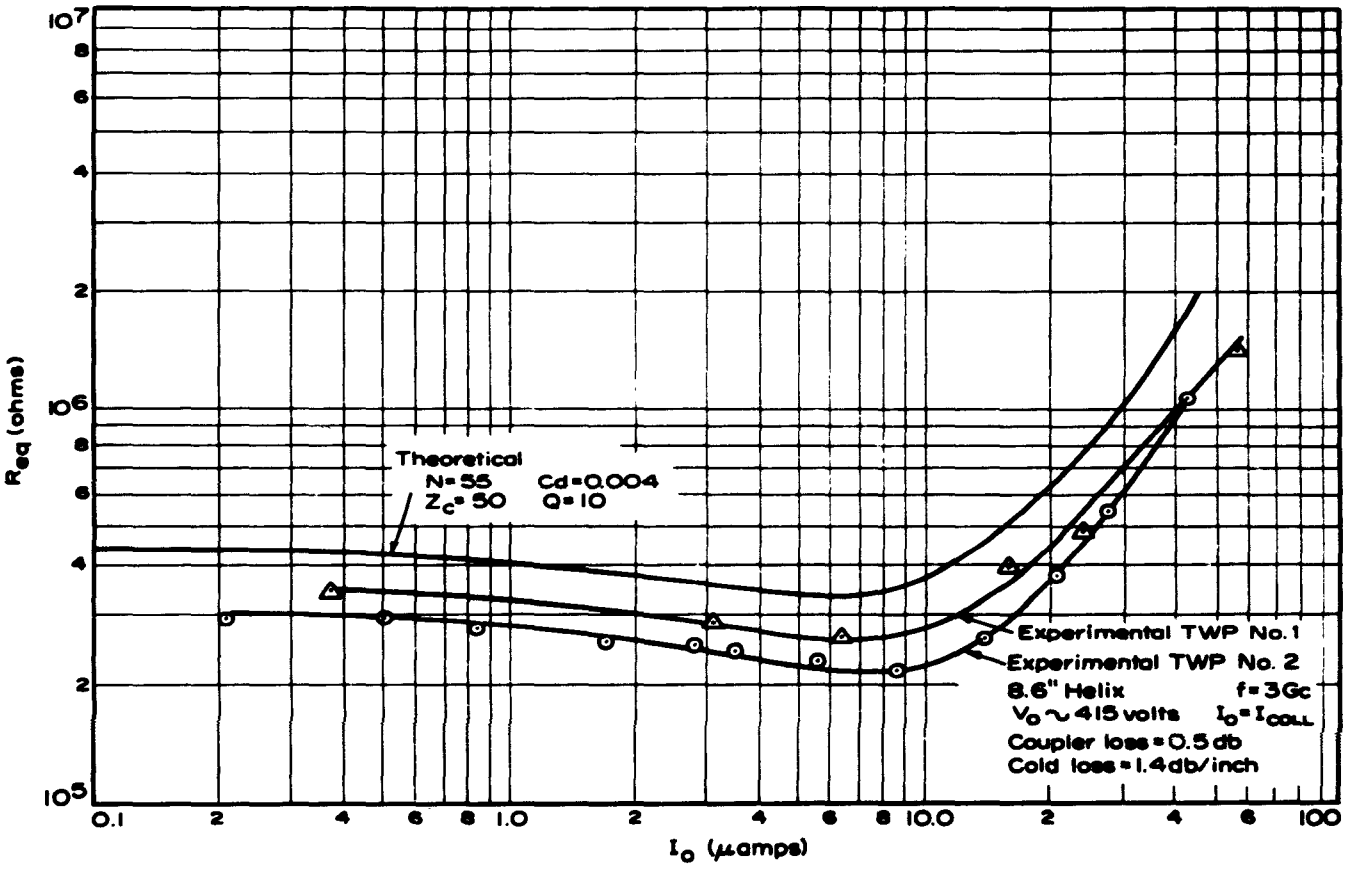

Figure 9. Comparison of Theoretical and Experimental Effects of Beam Current Level on TWP Equivalent Resistance

Interim Engineering Report No.3

RESEARCH ON TECHNIQUES FOR LIGHT MODULATION DETECTION

December 1, 1962 to March 1, 1963

D. E. Caddes
R. Targ
B. J. McMurtry

Contract AF 33(657)-8995

The applied research reported in this document has been made possible through support and sponsorship extended by the Electronic Technology Laboratory of the Aeronautical Systems Division, under Contract No. AF 33(657)-8995. It is published for technical information only, and does not necessarily represent recommendations or conclusions of the sponsoring agency.

MICROWAVE DEVICE DIVISION

SYLVANIA ELECTRIC PRODUCTS INC.

MOUNTAIN VIEW, CALIFORNIA

INTERIM ENGINEERING REPORT NO. 3

RESEARCH ON TECHNIQUES FOR LIGHT MODULATION DETECTION

December 1, 1962 to March 1, 1963

BPSN 6799

Contract AF 33(657)-8995

Prepared by

D. E. Caddes
R. Targ
B. J. McMurtry

Approved by

B. J. McMurtry, Head
Optical Devices Department

R. E. Hutter, Chief Engineer
Microwave Device Division

MICROWAVE DEVICE DIVISION
SYLVANIA ELECTRIC PRODUCTS INC.
500 Evelyn Avenue
Mountain View, California

ABSTRACT

This report covers the third quarter of an applied research program conducted by the Sylvania Microwave Device Division to establish techniques for light modulation detection.

A continuing theoretical and experimental analysis of light detection schemes has reaffirmed the conclusion that the traveling-wave microwave phototube is the most promising method consistent with the objectives of this program.

Progress is described in the following areas: (1) theoretical analysis of microwave phototubes; and (2) experimental measurements on microwave phototubes and other demodulators.

TABLE OF CONTENTS

TABLE OF CONTENTS (Cont.)

LIST OF ILLUSTRATIONS

GLOSSARY

ϕ = normalized forward circuit wave; circuit power = $2|\phi|^2$

σ = normalized slow space charge wave; slow space charge wave power = $2|\sigma|^2$

ρ = normalized fast space charge wave; fast space charge wave power = $2|\rho|^2$

Z = axial distance from helix input

β_e = ω/u_o = electron beam propagation constant

u_o = average electron velocity

ω = $2\pi f$ = radian frequency

ω_q = reduced radian plasma frequency = $R(\eta i_o/\epsilon_o u_o)^{1/2}$

R = plasma frequency reduction factor

i_o = beam current density (amps/meter^2)

ϵ_o = permittivity of free space = 8.85×10^{-12} farad per meter

b = Pierce velocity parameter

C = $(I_o Z_c/4V_o)^{1/3}$ = Pierce gain parameter

d = Pierce loss parameter

K = $(C^3\omega/2\omega_q)^{1/2}$ = beam-circuit coupling coefficient

I_o = average beam current

Z_c = longitudinal beam-circuit interaction impedance

V_o = d-c beam voltage

Z_b = $(2V_o\omega_q/I_o\omega)$ = beam impedance

η = electron charge to mass ratio or quantum efficiency

QC = Pierce space charge parameter

Q = Pierce passive mode parameter

v_p = cold circuit phase velocity

V_1 = a-c kinetic beam voltage

i = peak a-c current modulation

v = peak a-c velocity modulation

I_B = Background current

I_D = dark current

P_v = velocity fluctuation noise power output

P_t = thermal noise power output

P_s = shot noise power output

SECTION I

OBJECTIVE

The objective of this program is to conduct applied research on techniques for light modulation detection. Devices capable of detecting the modulation on a light signal are sought. Consideration will be given to the feasibility of including an amplification process for the detected signal.

SECTION II

TECHNICAL APPROACH

A continuing comparison of various light detection schemes has reaffirmed the conclusion that the microwave phototube is the most promising method of light modulation detection, consistent with the following desirable characteristics:

(a) Capability of detecting light signals modulated at microwave frequency rates;
(b) Capability of detecting with large modulation bandwidths (greater than 1 Gc);
(c) Suitability for optical heterodyne detection; and
(d) Capability of amplification in the light modulation detector.

The technical program reported here consists of two related areas:

(1) Theoretical analysis of microwave phototubes; and
(2) Experimental measurements on microwave phototubes and other light modulation detectors.

Very little effort was expended during this period on tube construction. Since tubes were available for the experiments, there was no need for building more tubes on this contract.

The progress in these specific areas will be described in the following sections.

SECTION III

THEORETICAL ANALYSIS OF MICROWAVE PHOTOTUBES

3.1 Objective

The objective of this investigation is to examine theoretically the power output, bandwidth, and noise of microwave phototubes.

3.2 Noise Analysis

The major sources of noise in microwave phototubes were examined in Interim Engineering Report No. 2. During this quarter we have been able to draw more firm conclusions concerning the importance of velocity fluctuation noise.

The mean square noise velocity modulation at the cathode is[1]

$$|v_N|^2 = \frac{2eB}{I}\,\overline{\delta v^2}$$

where I is the total photocurrent and $\overline{\delta v^2}$ is the variance or mean square deviation of the emission velocity. (Velocity fluctuation noise accompanying dark current has been neglected in this calculation).

In order to compute the noise velocity modulation at the helix input, one must construct a suitable noise kinetic voltage. Of the several possible choices[2], we will select a kinetic voltage based on the mean velocity at the cathode, $\bar{v}$. Then the noise kinetic voltage is $V_N = \bar{v} v_N / \eta$, and the noise power output due to velocity fluctuations is

$$P_v = \frac{2eB}{I}\,\frac{\bar{v}^2\,\overline{\delta v^2}}{\eta^2}\,G_{eq}$$

Then the over-all signal-to-noise ratio is

$$\frac{S}{N} = \frac{\frac{1}{2}|i|^2 R_{eq}}{P_T + P_s + P_V}$$

In many instances $I_o \gg I_\beta + I_D$, and the signal-to-noise ratio becomes

$$\frac{S}{N} = \frac{\frac{1}{2}|i|^2 R_{eq}}{kTB + 2eI_o B R_{eq}(1 + P_V/P_s)}$$

where

$$\frac{P_V}{P_s} = \pi^2 N^2 \frac{\overline{\delta v^2}}{u_o^2} \cdot \frac{\bar{v}^2}{u_o^2}$$

which is generally much less than unity; e.g., for a rectangular velocity distribution at the cathode,

$$\frac{P_V}{P_s} = \frac{1}{48} \pi^2 N^2 \left(\frac{v_{max}}{u_o}\right)^4$$

where v_{max} is the maximum velocity of electron emission. P_V/P_s is approximately 10^{-4} for the Sylvania SYD-4302A at $\lambda = 6328$A. (A similar calculation for velocity fluctuation noise due to dark current shows it to be negligible also).

Consequently the signal-to-noise ratio reduces to

$$\frac{S}{N} = \frac{\frac{1}{2}|i|^2 R_{eq}}{kTB + 2eI_o B R_{eq}}$$

Both noise power output and signal-to-noise ratio for the Sylvania SYD-4320A were presented in Interim Engineering Report No. 2 (Figures 6 and 7).

3.3 Gun Region Analysis

Some time was spent in examining the various ways of treating the microwave effects of the gun region at high current levels, but no conclusion was reached concerning what technique would be best suited to our problem. Further work will be reported in the next report.

3.4 Multivelocity Beam Analysis

Emitted photoelectrons may have initial energies as high as

$$E_{max} = h\nu - \phi$$

where h is Planck's constant, ν is the frequency of the incident light, and ϕ is the work function of the photocathode. At visible wavelengths this energy may be as high as one electron-volt, and the range of emission energies will be from zero to E_{max}. This means that the electron beam is not actually the single-velocity stream which is assumed in many analyses of gun region effects and beam-circuit interaction, but is actually a multi-velocity stream.

The consequences of having a multi-rather than single-velocity electron beam may be determined by use of the density-function method of analysis.[2] The problem separates rather naturally into two parts: (1) the gun or accelerating region; and (2) the beam-circuit interaction region. We have formulated the coupled-mode differential equations for the latter system for an assumed velocity distribution, and plan to examine the former during the next quarter. The complexity of the equations demands solution by the use of a high-speed digital computer. Because of the time and effort required to obtain such solutions, we are simplifying the equations in an attempt to obtain closed form solutions. Based on the simplified solutions, we will decide whether to carry out the more involved analysis.

3.5 Detailed Calculations of Equivalent Resistance

In Interim Engineering Report No. 2 we introduced a figure of merit for traveling-wave microwave phototubes (TWP's), the "equivalent resistance", defined by

$$P_{out} = \frac{1}{2} \; i^{2} R_{eq}$$

where P_{out} is the output power of the TWP and i is the peak a.c. current modulation on the photoelectron beam. R_{eq} is thus a transfer function which describes the efficiency of the beam-circuit interaction in producing circuit power output from an input consisting of current modulation on the beam. We are interested in current modulation inputs because this is the excitation typical of TWP operation at low to moderate average current levels. That is, an amplitude-modulated light beam is a number-modulated photon beam which, upon reaching a photocathode, produces a correspondingly number-modulated (current-modulated) photoelectron beam. This signal will be the input to the beam-circuit interaction region provided the average current is not too high. At high average currents there may be significant conversion of current modulation into velocity modulation as the beam moves from the cathode to the helix input (Section 3.3).

The coupled-mode differential equations describing the small-signal coupling between an electron beam and a slow-wave circuit, including the effects of space charge, asynchronous beam velocity, circuit loss, and finite C are[3]

$$\left[\frac{d}{dz} + j\beta_e (1 + Cb - j Cd)\right]\phi = K \frac{d}{dz}(\rho - 6)$$

$$\left[\frac{d}{dz} + j\beta_e \left(1 + \frac{\omega_q}{\omega}\right)\right] 6 = K \frac{d}{dz}\phi$$

$$\left[\frac{d}{dz} + j\beta_e \left(1 - \frac{\omega_q}{\omega}\right)\right] \rho = K \frac{d}{dz}\phi$$

where the symbols have been defined in the glossary. The backward circuit wave has been neglected since its transfer coefficient with the other waves is small for all cases of interest.

Simultaneous solution of these three equations results in expressions for ϕ, 6, and ρ in terms of the sums of three waves whose Z-direction propagation constants are functions of the space-charge conditions, beam velocity, circuit loss, and beam-circuit coupling. The amplitudes depend both upon these parameters and upon the boundary conditions at Z= 0. For example,

$$\phi = A_1 e^{\gamma_1 z} + A_2 e^{\gamma_2 z} + A_3 e^{\gamma_3 z}$$

The A_n and γ_n are complex numbers and are, in general, complicated functions of the tube parameters and boundary conditions. By programming the solutions for the IBM 7090 high-speed digital computer, we have made possible the rapid calcuation of the effects of varying the parameters over wide ranges, with arbitrary boundary or excitation conditions.

For typical TWP operation, the excitation is pure current modulation,

$$i(6) = 2 Z_b^{-1/2} [6(o) - \rho(o)]$$

$$6(o) = -\rho(o)$$

$$\phi(o) = 0$$

and the output power is

$$P_{out} = 2|\phi|^2 = 1/2 |I|^2 R_{eq}$$

Upon rearrangement this yields

$$\frac{R_{eq}}{Z_c} = \frac{\omega_b}{2\omega C^3} \frac{|\phi|^2}{|G(o) - P(o)|^2}$$

Since the beam-circuit interaction impedance, Z_c, is a constant for a given circuit, frequency, and beam-circuit geometry, this ratio is a convenient normalization of R_{eq}. By setting

$$G(o) = -P(o) = \tfrac{1}{2},$$

we can use the solution for the circuit wave amplitude, ϕ, to calculate R_{eq}/Z_c.

Before discussing the results of our computations of R_{eq}/Z_c, a few comments on the tube parameters[4] are in order:
The velocity parameter "b" is defined by

$$\frac{V_o}{V_s} = (1 + Cb)^2$$

where V_o is the operating beam voltage and V_s is the synchronous voltage, corresponding to the phase velocity of the circuit alone:

$$v_p = (2\eta V_s)^{1/2}$$

The gain parameter C is

$$C = \left(\frac{Z_c I_o}{4 V_o}\right)^{1/3}$$

Q, the passive mode parameter, describes the effects of circuit modes other than the fundamental. It is determined primarily by the circuit configuration and the beam-circuit geometry and is nearly constant for a given circuit, frequency, and beam-circuit geometry. Its part in space-charge effects is described by

$$(4QC^3)^{1/2} = \frac{\omega_q}{\omega + \omega_q}$$

Using the definitions of C and the fact that Z_c is independent of the beam current level and beam voltage, this becomes

$$Q = \text{Const.} \times \frac{V_o^{1/2}}{(\omega + \omega_q)^2}$$

For typical TWP operation, $\omega >> \omega_q$ and V_o varies only a few per cent as I_o changes, so we may assume Q approximately constant.

Circuit loss is related to Cd by

$$Cd = 0.0183 \frac{L}{N}$$

where L is the circuit cold loss in decibels and N is the circuit length in wavelengths. A typical value of 0.004 has been used in the figures which follow.

Figures 1 and 2 show how R_{eq} varies as a function of beam velocity. One of the most important features of these data is the narrowing of the curves with increasing circuit length. This means that the value of the helix voltage is more critical for longer tubes. Another interesting effect is that Q becomes more important as the curves narrow. Space-charge effects also shift the optimum value of b away from zero, as is seen in Figure 2.

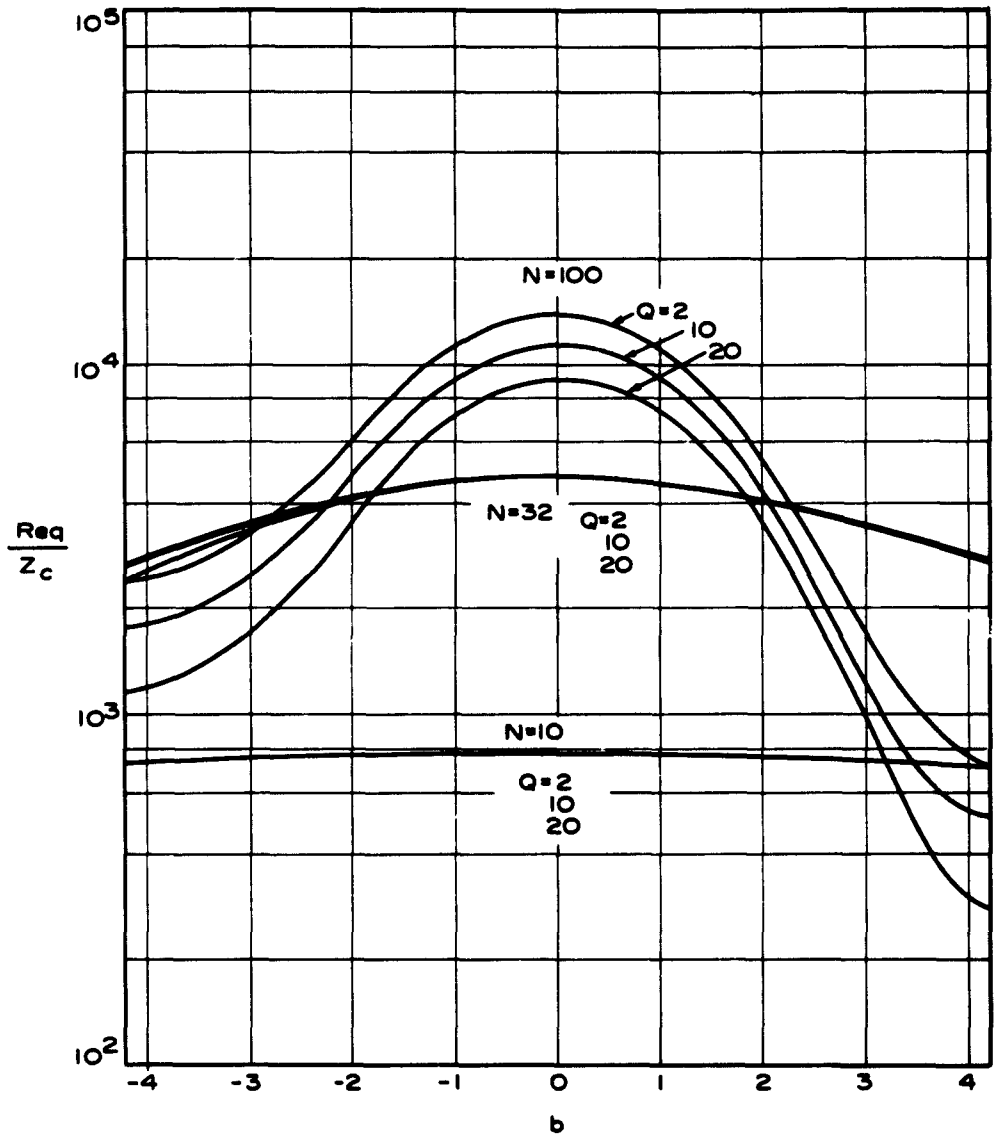

Figure 1. Effect of Beam Velocity Variations on TWP Equivalent Resistance.
C = 0.003; Cd = 0.004

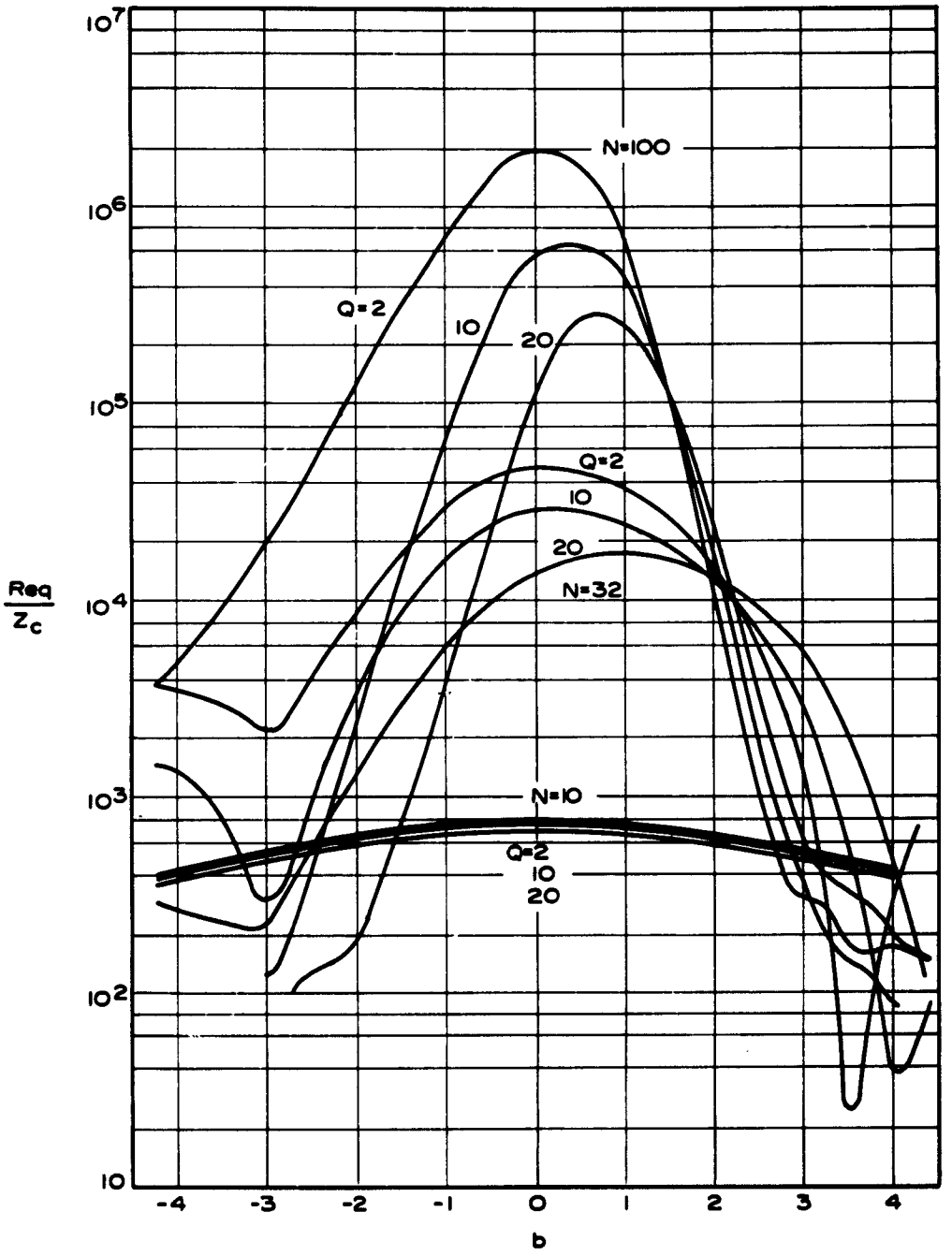

Figure 2. Effect of Beam Velocity Variations on TWP Equivalent Resistance
C = 0.010; Cd = 0.004

These results agree with intuition: a short length of circuit should be less sensitive to beam velocity because it is not necessary to maintain the proper phase between the exciting signal on the beam and the circuit wave for as long a period as with a longer circuit. The longer tube will deliver more output power because it is coupled to the beam longer and can take more energy from it. Space-charge effects become more important because they act over a longer period.

Figure 3 displays the dependence of R_{eq} on the gain parameter C. For very small C, the equivalent resistance is constant for a given circuit, as predicted by the simpler theory reported in Interim Engineering Report No. 2, but when C is increased sufficiently (by raising the beam current and/or the interaction impedance), a region of higher R_{eq} is reached. In this range of C, one of the three waves which comprise the circuit wave, the one corresponding to the "growing wave" of traveling-wave tubes theory, has become significantly larger than its companions. It is, additionally, growing exponentially with distance, while one is losing power due to the circuit loss and another due to both the beam and the circuit loss. From Figure 3 it is seen that the value of C required for operation in this "exponential growth region" depends upon the length of the circuit employed; we see that the region begins near CN = 0.4. This graph is most useful in predicting the R_{eq} a given circuit will provide at various current levels.

Space-charge effects are again apparent, with the interesting result that they become important only as C approaches the values for growing wave operation. A consequence of the space-charge

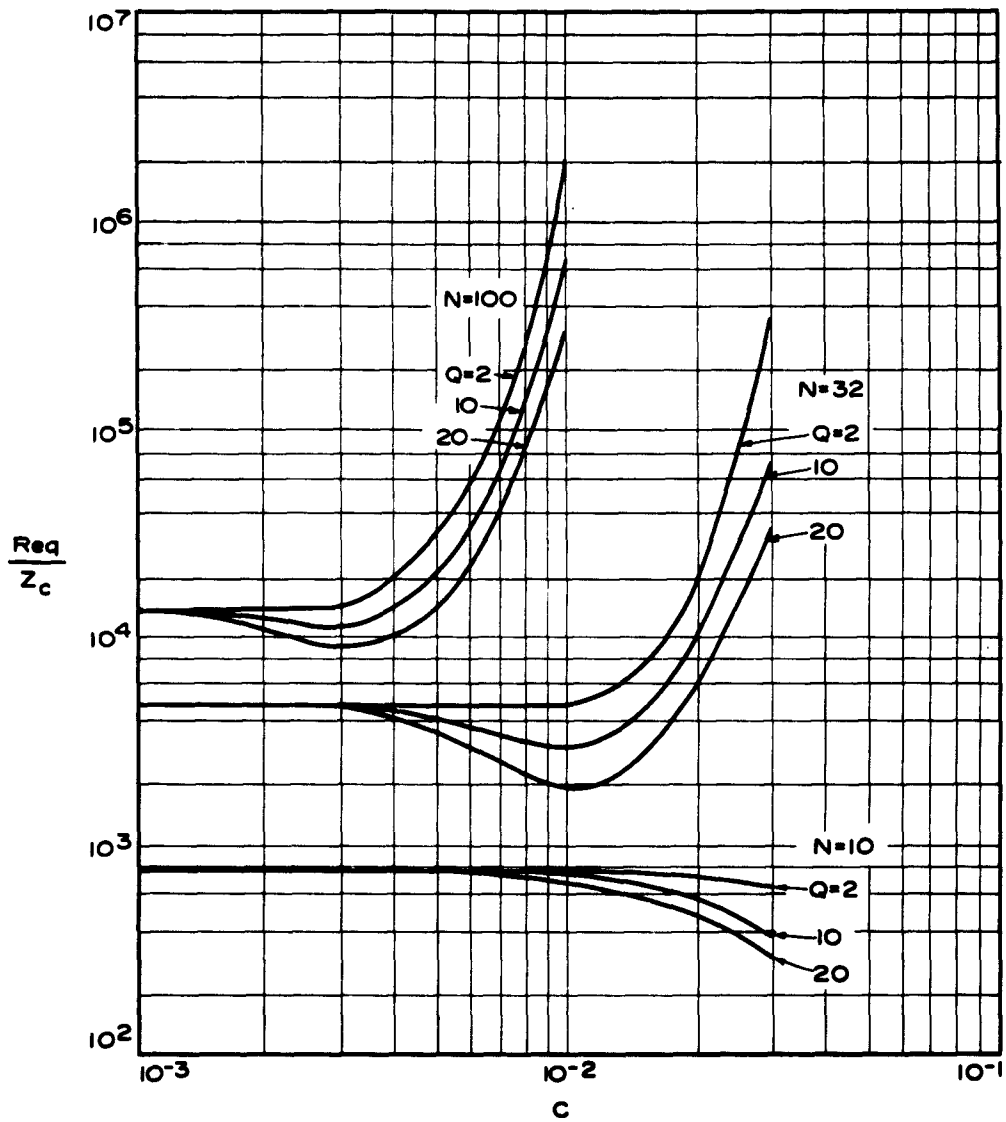

Figure 3. Dependence of TWP Equivalent Resistance upon the Pierce gain Parameter, C.
Cd = 0.004; b = optimum value for each C, N, Q

effects is that raising C (e.g., by raising the current level) for a circuit with Q = 10 or 20 decreases R_{eq} for a certain range of C. If the a.c. current modulation remains constant while the average current level is thus raised, a decrease in power output will result. If, however, the modulation index remains constant, the power output will go up, since it varies as the square of the initial a.c. current.

In Figure 4 is shown the way in which R_{eq} varies with circuit length for various values of C. For small N (CN less than about 0.3) we observe that R_{eq}/Z_c is proportional to N^2, as predicted by the simpler theory reported in Interim Engineering Report No. 2. As N is increased beyond $CN \cong 0.4$, the growing wave operation begins and R_{eq}/Z_c varies as exp(N). This graph is useful in designing a TWP for operation at specific current levels because it indicates the circuit length required for a given R_{eq}. Since the power output varies directly with R_{eq}, it would be advantageous to make the circuit long enough to reach the exponential growth region, if this is a reasonable length.

Space-charge effects again manifest themselves, but, at least for values of Q of 20 or less (typical of TWP's), an increase in circuit length does not result in a decrease in R_{eq} and power output. Larger Q's are unlikely in practice, but would result in a region where increasing the tube length would decrease R_{eq} and the power output.

We have kept the circuit loss constant in these curves in order to minimize curve-lotting. Loss is extremely important, however, as may be seen in Figure 5, which shows how it affects R_{eq} for

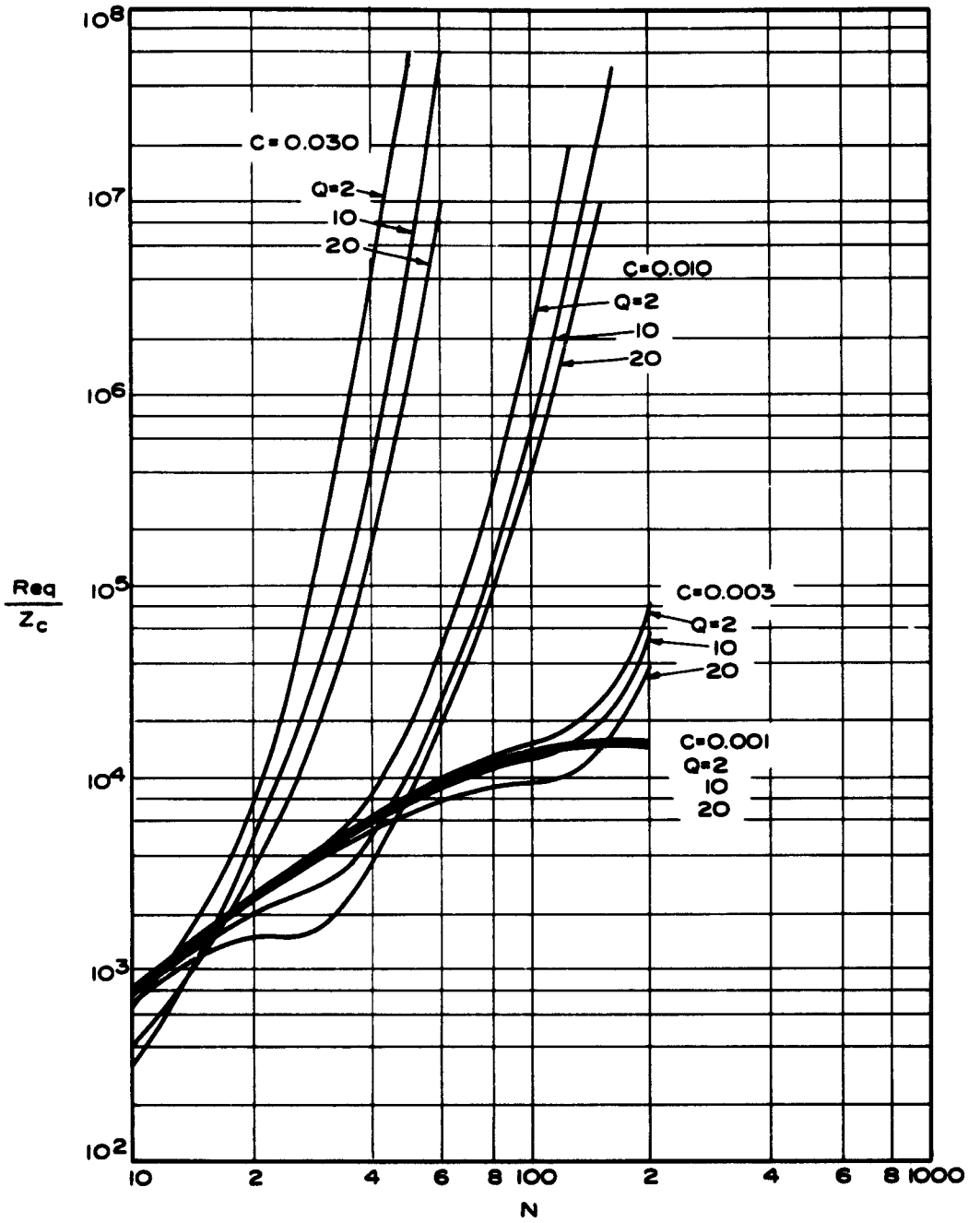

Figure 4. Dependence of TWP Equivalent Resistance upon Circuit Length
Cd = 0.004; b = optimum value for each C,N,Q

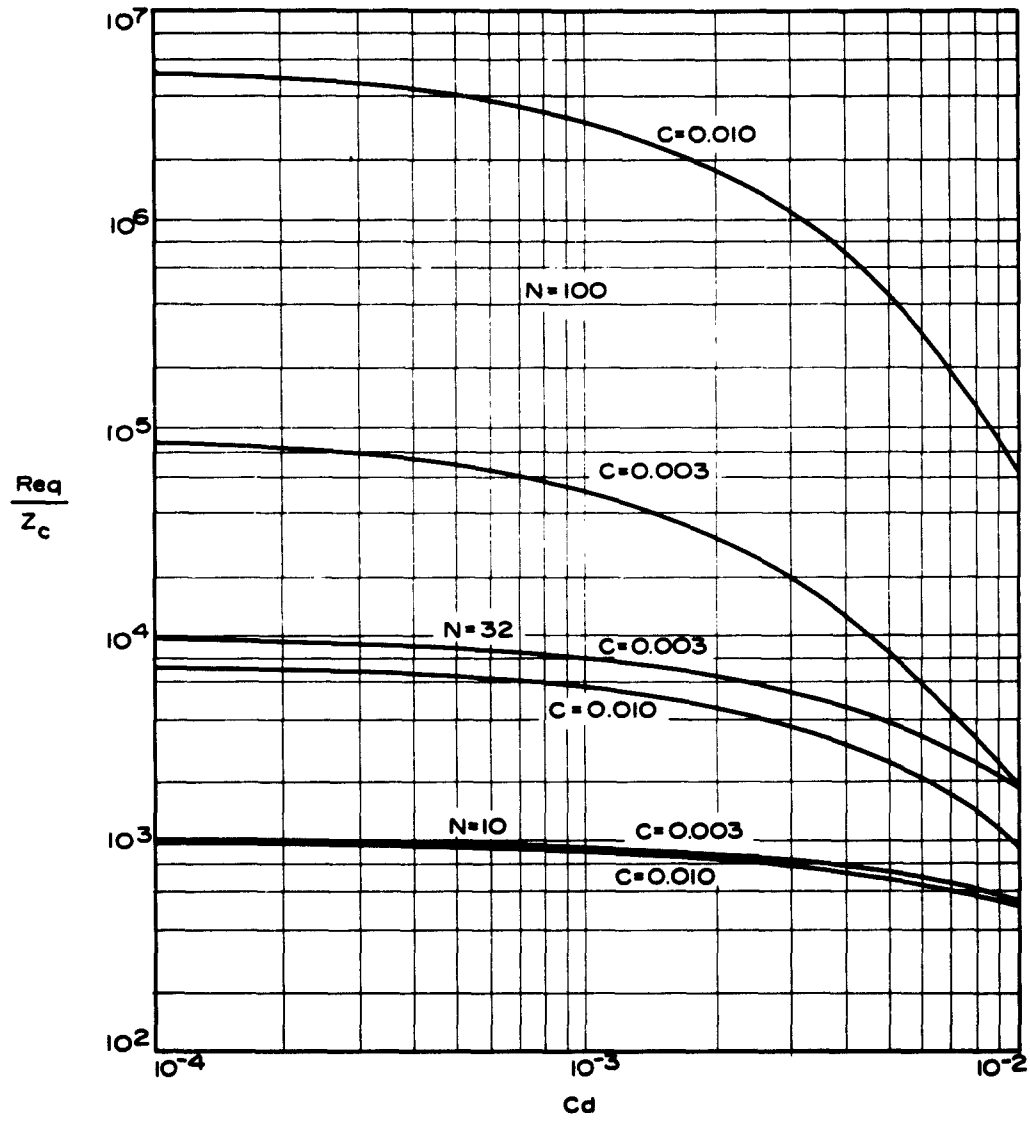

Figure 5. Effect of Circuit Loss on
TWP Equivalent Resistance.
Q = 10; b = optimum value for each C, N

various N and C. In general, the longer the circuit, the more severely performance is affected by loss.

In discussing the "growing wave" region, we alluded to the operation of traveling-wave tubes. The differential equations presented earlier describe the TWT also; the only difference (and a significant one) from the TWP case is that the excitation is applied to the circuit, rather than to the beam. The TWT boundary conditions are thus

$$b(0) = p(0) = 0$$

$$\phi(0) = \tfrac{1}{2} P_{in}$$

At the low currents typical of TWP operation, a TWT demonstrates net loss rather than gain, but begins to evidence some "response" for sufficiently long circuits. Figure 6 compares the beam velocity dependence characteristics of a TWP and a TWT at $C = 0.003$, which is a respectable TWP operating level. The TWT curves show very little beam-circuit interaction for $N < 40$, while the TWP responds at $N = 10$. The reason is that a current-modulated beam, which the TWP has, is in the optimum form for interacting with a circuit. It will induce a significant signal even in a very short length of circuit. The TWT's input circuit wave, however, must first velocity-modulate the beam, requiring circuit length; the velocity modulation then drifts into current modulation taking more length, and the beam is finally ready to begin efficient excitation of the circuit.

3.6 Detailed Calculation of Equivalent Conductance

Two types of excitation of the beam-circuit system have been discussed in the previous section: the pure current modulation

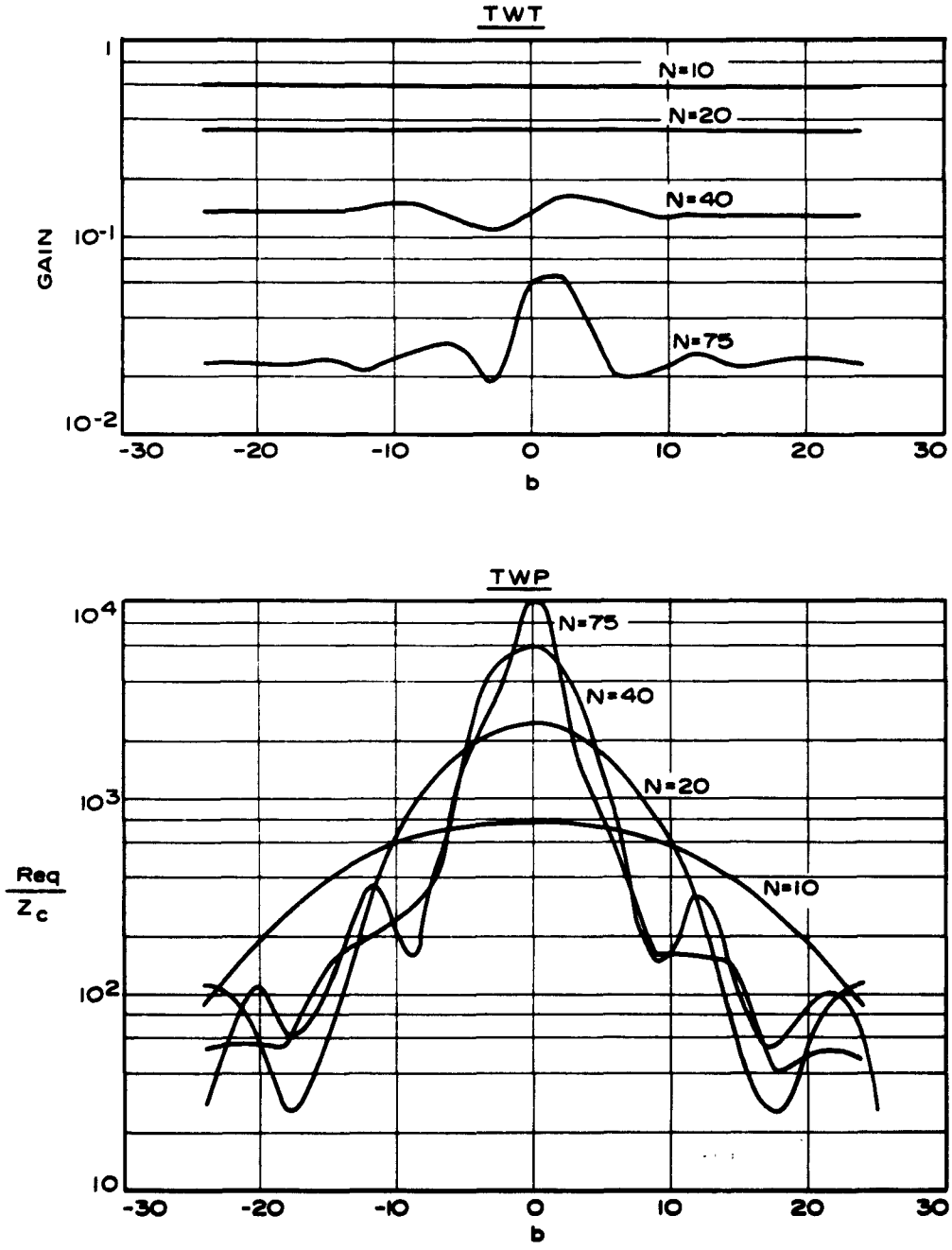

Figure 6. Comparison of TWT and TWP Response to changes in Beam Velocity. C = 0.003; Cd = 0.004; Q = 10

input and the pure circuit power input. A third possibility is pure velocity modulation of the electron beam. This type of excitation can result from passing the beam through a klystron gap, where time-varying electric fields velocity-modulate the electron stream, from emission velocity fluctuations at the cathode, or from letting a current-modulated beam drift a quarter of a plasma wavelength.

An equivalent conductance which describes the efficiency of the beam-circuit system in producing circuit power output from a velocity-modulation input may be defined by

$$P_{out} = \tfrac{1}{2} |V_1(0)|^2 G_{eq}$$

where V_1 is the a.c. kinetic beam voltage, related to the peak velocity modulation by

$$V_1 = \frac{u_0}{\eta} v(0)$$

The appropriate boundary conditions for this type of excitation are

$$V_1(0) = 2 Z_b^{1/2} \left[G(0) + \rho(0) \right]$$

$$G(0) = \rho(0)$$

$$\phi(0) = 0$$

By the same sort of rearranging done with R_{eq} in the previous section, we can normalize G_{eq} to the interaction impedance Z_c:

$$G_{eq} Z_c = \frac{2C^3\omega}{\omega_q} \quad \frac{|\phi|^2}{|G(0) + P(0)|^2}$$

If we choose $G(0) = P(0) = 0.5$ as our boundary conditions, we can easily compute the product $G_{eq} Z_c$ from the computer solution for ϕ.

These calculations have been performed for the same range of parameters used in the R_{eq}/Z_c data and are presently being plotted. The resulting curves will be presented in the next report.

3.7 Conclusions

An analysis employing the coupled-mode formulation of the traveling-wave microwave phototube beam-circuit interaction problem has led to a better understanding of TWP characteristics. The data obtained will permit more accurate predictions of the power output under given conditions and will enhance tube design.

Some of the more important observations resulting from this analysis are:

1) The mode width (i.e., the range of helix voltage over which the power output is within 3 db of its maximum value) narrows as the circuit length increases.
2) Space-charge effects raise the optimum helix voltage as the beam current is increased.
3) For a given current level, space-charge effects reduce the equivalent resistance of tubes which are long enough or nearly so for "growing wave" operation, but may be neglected for shorter tubes.
4) In the growing wave region, increases in average current produce large increases in R_{eq}.
5) Increases in average current, in the range just below that for growing wave operation, produce decreases in R_{eq}; below

this range R_{eq} is independent of the average current level.

6) R_{eq} increases with increasing circuit length for values of the passive mode parameter less than 20, but larger Q's can result in a range for which increasing the circuit length decreases R_{eq} and thus the power output.
7) Increasing the circuit loss lowers the R_{eq} of longer tubes more severely.
8) At typical TWP current levels, a system operated as a TWT shows significant beam-circuit interaction only for circuit lengths nearly an order of magnitude larger than those required of the same system used as a TWP.

Detailed analysis of the case of velocity-modulation input should further improve our understanding of the beam-circuit system.

The TWP analysis we have performed assumes a single-velocity electron beam. Actually, initial velocity effects result in a multi-velocity stream, with the range of velocities determined by the range of electron emission energies. This will affect both gun region effects and beam-circuit interaction.

Finally, an analysis of the microwave effects in the gun region at high average current levels should complete the theoretical treatment of the microwave phototube.

3.8 Plans for the Next Period

The program for the next period is as follows:

(1) Continue the gun region analysis with emphasis on high average current operation;
(2) Complete the analysis of the G_{eq} calculations, and summarize the results; and
(3) Continue the multi-velocity beam analysis.

SECTION IV

EXPERIMENTAL ANALYSIS OF MICROWAVE PHOTOTUBES AND OTHER LIGHT DEMODULATORS

4.1 Objective

The purpose of this investigation is to examine experimentally the power output, bandwidth and noise in microwave phototubes and other light demodulators.

4.2 Measurements on SYD-4302A TWP's

4.2.1 Power Output

The construction and operation of a complete c-w microwave modulation-demodulation experiment were described in Section V of Interim Engineering Report No. 2. During this quarter the experiment was refined to permit power measurements with better than 30 db signal-to-noise ratio in a 100 cycle bandwidth without the use of a phase-sensitive detector.

Typical experimental results for the SYD-4302A are presented in Table 4.2.

TABLE 4.2

Typical Experimental Results on SYD-4302A

Modulation index, m	12%
Average photocurrent, I_o	0.42 μamp
Modulation frequency, f	3.15 Gc
Microwave power output, P	-73 dbm
a.c. photocurrent, $i = mI_o$	0.05 μamp
"Measured" $R_{eq} = 2P/i^2$	40 KΩ

R_{eq} computed from simplified theoretical analysis	87 KΩ
Quantum efficiency	0.2%

Similar results were obtained on approximately ten other tubes. Since the simplified theory of Interim Engineering Report No. 2 neglected helix and coupler losses, the measured power output should be a few db less than the calculated value. For this tube the insertion loss of the helix plus output coupler is about 3 db, which can account for the difference between the measured and calculated power output.

Figure 7 shows measured and calculated power output as a function of the a.c. current modulation at the cathode, and the agreement is reasonably good. Some of the variation of the experimental curve from square-law growth can be attributed to the changes in beam geometry and position produced by increasing the average current under fixed magnetic field conditions.

Comparisons of TWP power output with the detailed theory of Section III are presented in Section 4.4.

4.2.2 Noise

The noise performance of the tube was examined by replacing the microwave modulator by a 1 Kc mechanical chopper and employing phase-sensitive detection of the TWP output. This permitted a direct measurement of the noise power output produced by light incident on the photocathode, since thermal noise and dark current noise were unmodulated and hence not detected. For an average current of 0.8 μamp and a receiver bandwidth of 3 Mc, the measured noise power output was -103 dbm. According to the

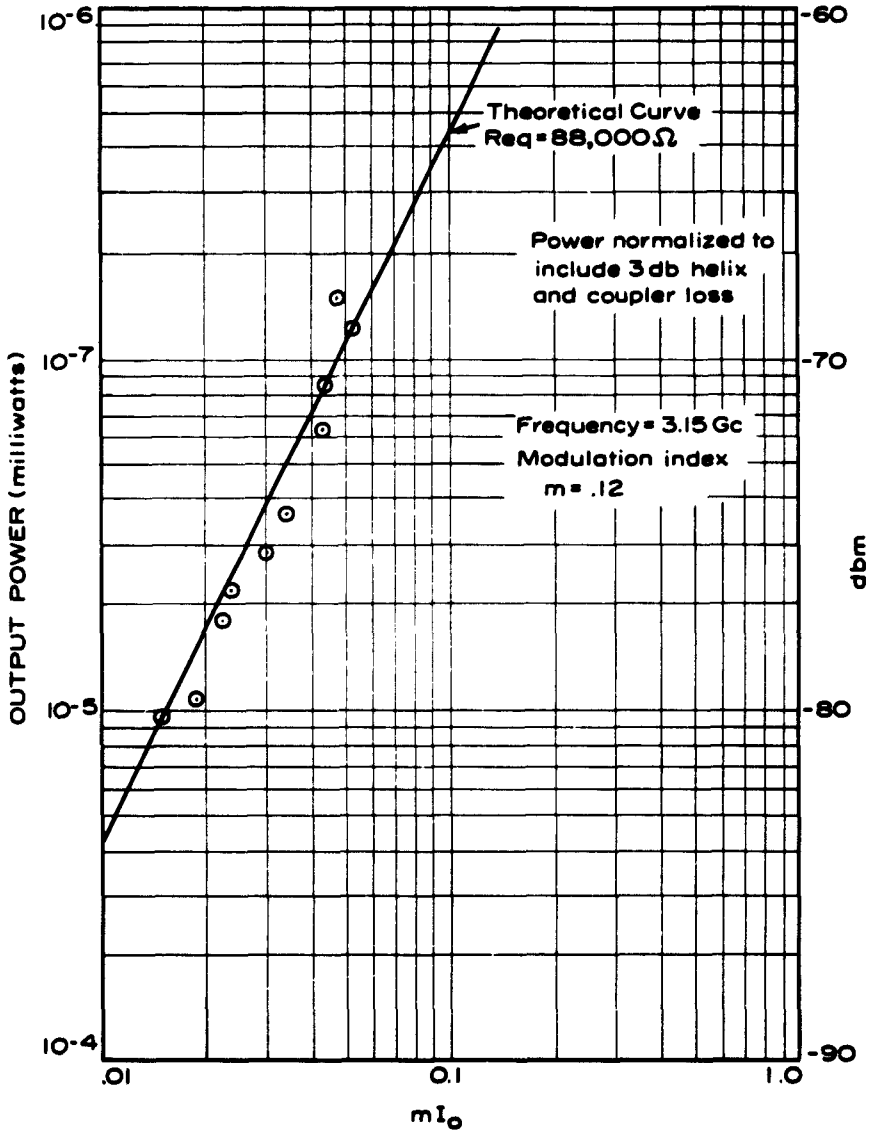

Figure 7. Comparison of Theoretical and Experimental TWP Equivalent Resistances.

theory of Section 3.2, the theoretical noise power output is the shot noise, $2eI_oBR_{eq}$; and from Figure 6 in Interim Engineering Report No. 2 its value should be -102 dbm. Subtracting the 3 db helix plus coupler loss from this figure yields a calculated noise power output of -105 dbm. It therefore appears that shot noise is the dominant light-dependent noise source in the tube.

More details of shot noise measurements are presented in Sections 4.3 and 4.4.

4.3 Techniques for Measuring R_{eq}

Theoretical analysis supported by the experiments described in the previous section indicates that: (1) the microwave power input of a TWP can be expressed as $P = 1/2\ m^2I_o^2R_{eq}$; and (2) the major light-dependent noise source is shot noise, which can be expressed as $P_s = 2eI_oBR_{eq}$. All of the quantities in each of these equations, with the exception of R_{eq}, can be measured directly, so that each equation provides an independent measurement of R_{eq}. Thus, one can measure R_{eq} either by performing a microwave modulation-demodulation-experiment or by modulating the light at a low frequency rate and performing synchronous detection of the noise power output. Of the two techniques the latter is the best suited to continuous frequency response measurements since one can simply tune his receiver across the desired frequency range. The relatively small bandwidth and tunability of currently available light modulators make it difficult to perform frequency response measurements using the modulation-demodulation technique.

4.4 Measurements on TWP's With Longer Helices

4.4.1 Introduction

In order to obtain a better understanding of the TWP we made measurements on tubes that could be readily operated on the exponential growth region. In the new tubes (made available to this project by a Sylvania-sponsored project) the active helix length was changed from 2 to 8 inches so that the tube would operate in the exponential growth region at a lower value of average current (e.g., at 10 μamp rather than at 1 mA).

Measurements of R_{eq} as a function of average current, helix voltage and frequency were performed using the shot noise measurement technique. The experimental arrangement is diagrammed in Figure 8. The light was chopped at 1 Kc by a rotating apertured disc. The output power from the TWP went to an S-band mixer crystal and then to a 30 Mc i-f amplifier having a 3 Mc bandwidth. The i-f output was detected with a lock-in amplifier, which derived its reference signal from a second light source and photocell adjacent to the chopping wheel. The sensitivity of the system was -117 dbm when the recorder time constant was one second. Absolute power measurements were made by substituting a calibrated S-band generator for the tube output and adjusting it to produce the same meter reading as the tube. The oscillator was gated by the same reference signal that was fed to the lock-in amplifier.

Experimental results on two tubes are presented in the following paragraphs.

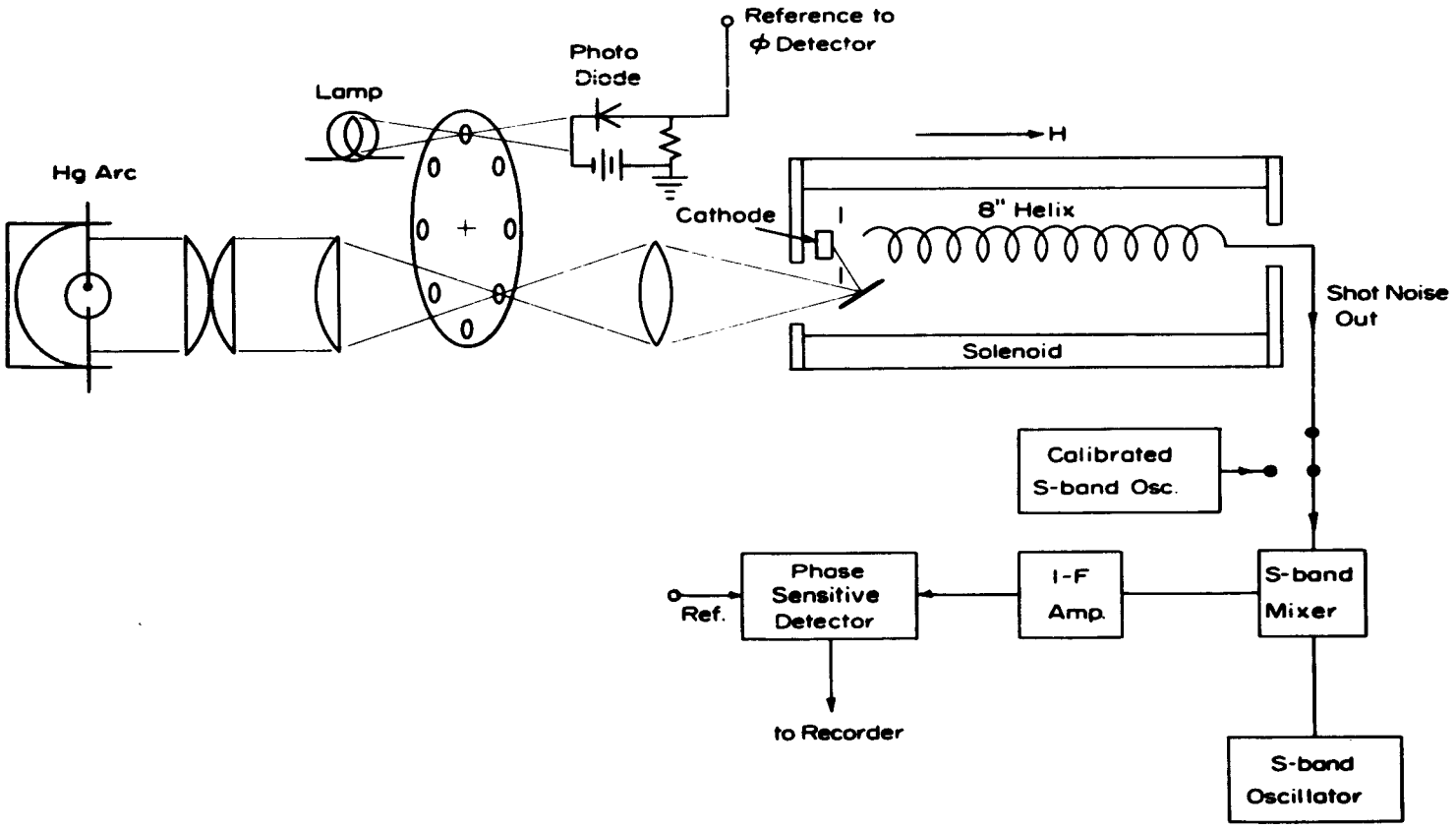

Figure 8. Apparatus for TWP Shot-Noise Measurement.

4.4.2 Variation of R_{eq} With Average Current

The shot noise power output near 3 Gc was measured for average currents between about 0.1 and 100 μamp. Corresponding values of R_{eq} were computed using a bandwidth of 3 Mc and an average current equal to the cathode current. The electron beam transmission was about 75% for each tube.

The experimental curves are plotted in Figure 9 along with a theoretical curve obtained from the detailed computer calculation. The general behavior of the theoretical prediction is certainly observable in the experimental curve. That is, R_{eq} is constant at low currents, then dips and rises rapidly as the current is increased.

Some of the difference btween the theoretical and experimental curves can be accounted for by the 0.5 db coupler loss that was not included in the calculation. Further investigation is continuing in an effort to determine just how well the curves could be expected to agree. One partial explanation of the difference in the shape of the curves is that the experiments were performed with a constant magnetic focusing field, which means that the average beam diameter increases with increasing current, whereas the calculation assumed a constant and uniform beam diameter.

Further comparisons will be presented in the next report.

4.4.3 Variation of R_{eq} With Helix Voltage

The shot noise power output near 3 Gc was measured as a function of helix voltage for several values of average current. The mode width (i.e., the range of voltage over which the power output is within 3 db of its maximum value) can be measured directly

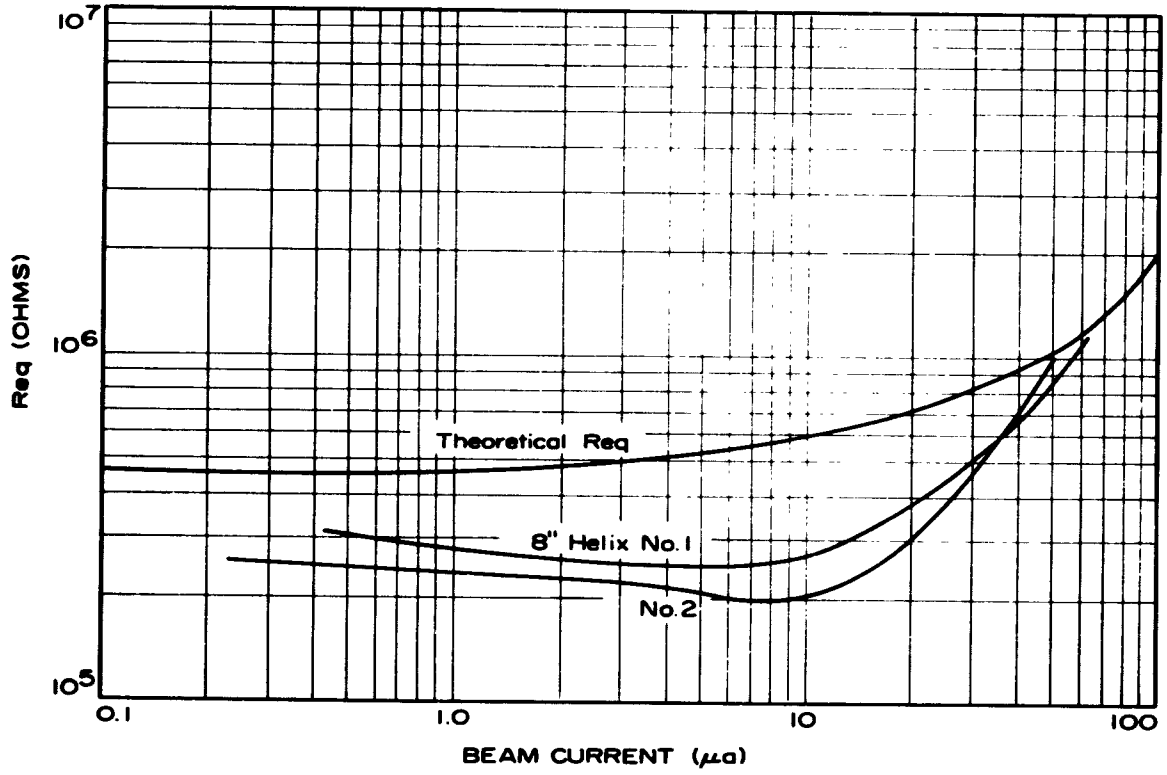

Figure 9. Comparison of Theoretical and Experimental Effects of Beam Current Level on TWP Equivalent Resistance.

from Figures 10 and 11, which show noise power output versus helix voltage for each tube.

As predicted by theory (Section III), both the mode width and the voltage for maximum power increase with increasing average current.

Similar measurements were also performed on a conventional tube with a 2 inch active helix length. Again as predicted by theory, the mode width was found to increase as the helix length was decreased.

More complete measurements and quantitative comparisons with theory will be presented in the next report.

4.4.4 Variation of R_{eq} With Frequency

The shot noise power output was measured as a function of frequency for several values of average current. As predicted by theory, R_{eq} appears to decrease monotonically with increasing frequency.

Detailed experimental results and quantitative comparison with theory will be presented in the next report.

4.4.5 Conclusions

Initial measurements on two tubes over a wide range of average current, helix voltage and frequency show good qualitative agreement with the theoretical predictions of Section III. Further experiments and specific calculations must be performed before conclusions can be drawn concerning the quantitative agreement.

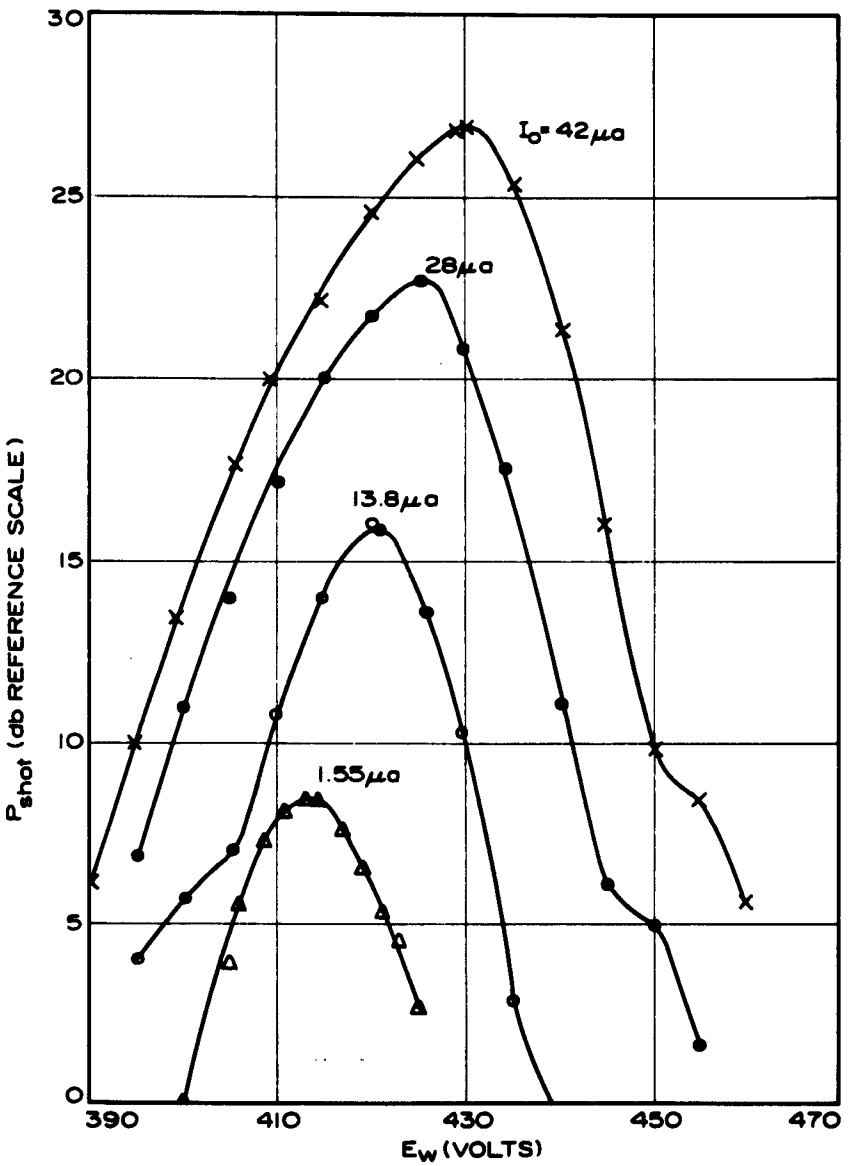

Figure 10. TWP Helix Mode Width,
8-inch Helix at 3 Gc.

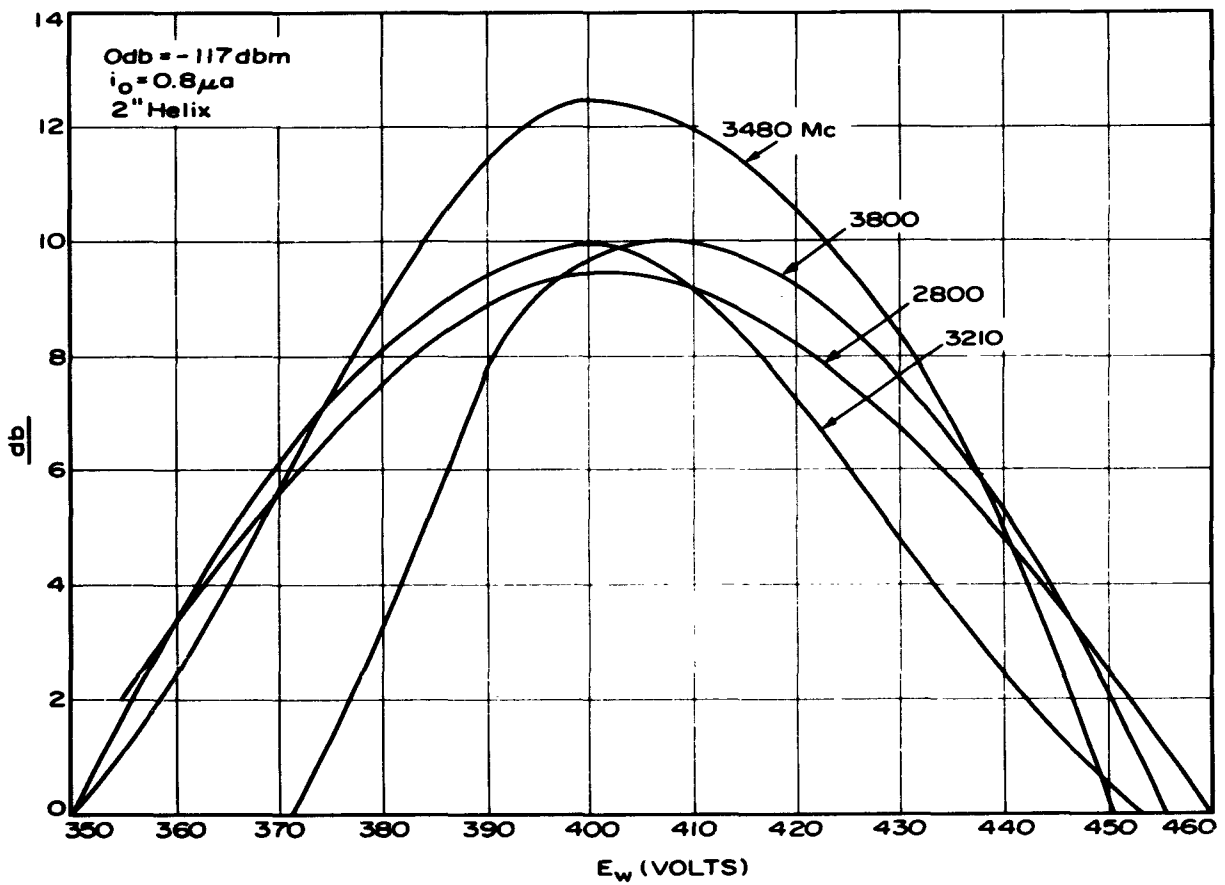

Figure 11. TWP Helix Mode Width, 2-inch Helix.

4.5 Direct Comparison of Several Light Demodulators

4.5.1 Introduction

Although theoretical comparisons of various light demodulators were presented in Interim Engineering Reports No. 1 and No. 2, no direct experimental comparisons have been reported. Consequently it was decided to perform a direct experimental comparison of: (1) solid-state photo-diodes[5-7]; (2) demodulators using bulk effects in cadmium selenide[8]; and (3) traveling-wave microwave phototubes.

Since the power output of each of these devices can be expressed as $P = 1/2\ m^2 I_o^2 R_{eq}$, a convenient figure of merit for comparing the devices is $\eta^2 R_{eq}$, where η is the quantum efficiency. The quantum efficiency can be directly computed from a knowledge of the average photocurrent and the incident light power, and R_{eq} can be computed from the above expression for microwave power output. In this formulation R_{eq} represents the over-all interaction efficiency and includes all factors affecting power output (e.g., possible transit time reduction factors, etc.).

The experimental arrangement was the S-band modulation-demodulation experiment diagrammed in Figure 12. In some measurements phase-sensitive detection was required, and an experimental arrangement like that shown in Figure 8 was used (however, the He-Ne laser rather than the mercury arc lamp was used as a light source). The light source was a He-Ne laser producing about 2 mw of output power at 6328Å. Demodulators could be inserted, tested and removed without any adjustments being made to the other parts of the optical or microwave system.

Experimental results are presented in the following paragraphs.

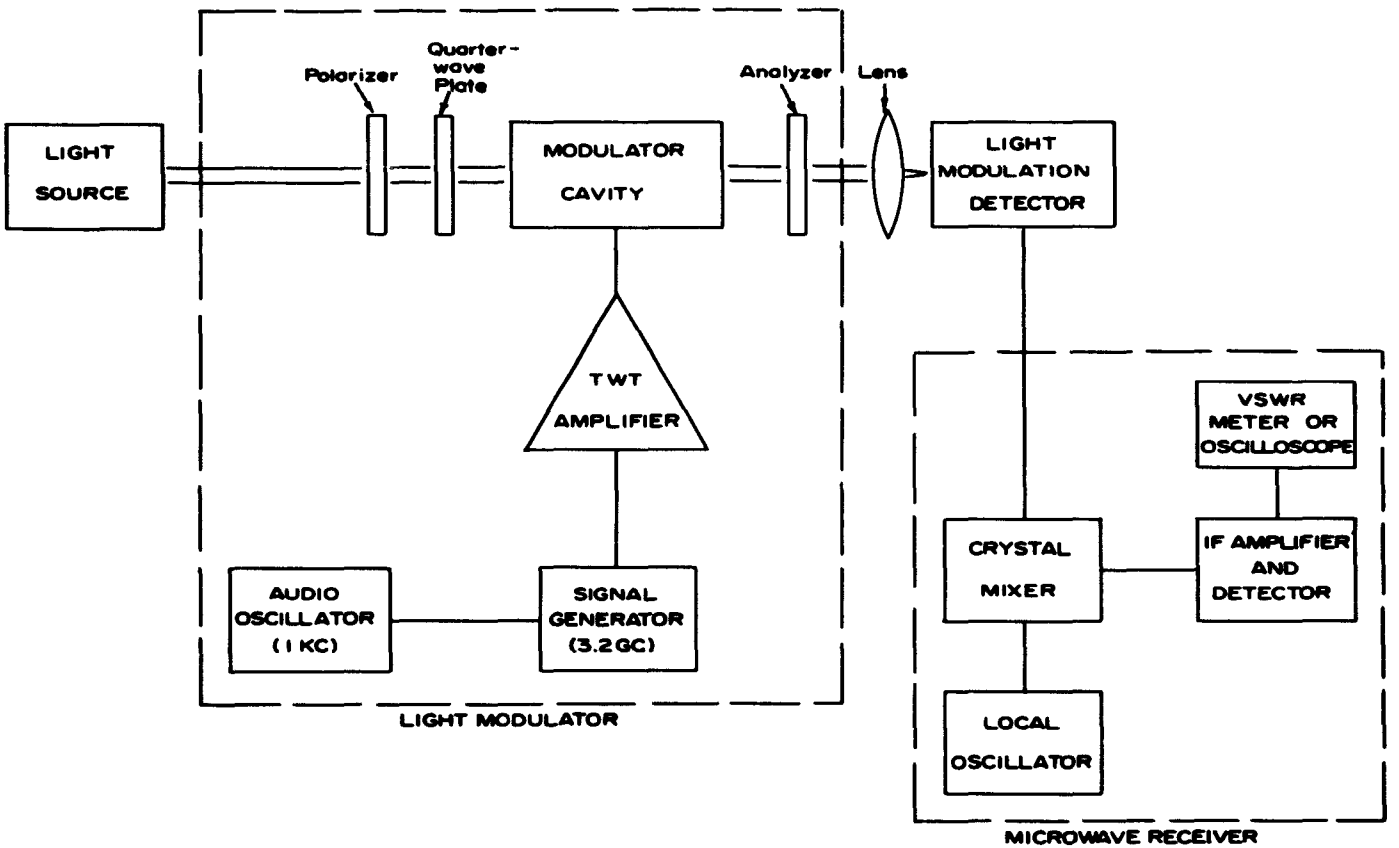

Figure 12. Modulation-Demodulation Apparatus.

4.5.2 Solid State Photodiodes

High-speed photodiodes similar to those described in the literature[5-7] were made available by Prof. A. E. Siegman and Mr. W. Huntley of Stanford University. One diode was fabricated by Prof. J. F. Gibbons and Dr. P. Prehn of Stanford University and the other was a commercially available Philco L4501 diode.

Since the active area around the perimeter of each diode was much less than 1 sq. mm the light had to be very carefully focused; and as a consequence of the small active area, it was difficult to estimate the amount of incident light that actually produced photocurrent. Although this geometrical difficulty casts doubt on the estimates of quantum efficiency, it does not affect the calculation of R_{eq}, which is computed simply from the readily measurable values of microwave power output and the average photocurrent.

With both diodes it was apparent that the regions of the perimeter which showed the highest quantum efficiency were not the regions giving the greatest microwave power output.

The highest microwave power output obtained was -70 dbm from the Philco diode and corresponded to R_{eq} = 3 ohms. The estimated quantum efficiency was 50 $\pm$ 20%, so that $\eta^2 R_{eq}$ was between 0.3 and 1.5 ohms. In all measurements on the diodes double-stub tuners were used to maximize the microwave power output.

4.5.3 Demodulators Using Bulk Effects in Cadmium Selenide

During this quarter a new light demodulator was described by DiDomenico et al[8]. It consists of a piece of CdSe placed in a waveguide or a cavity resonator. A d-c bias is provided between ohmic contacts on two opposite faces of the sample. Beats between

axial modes in a ruby laser were observed at substantial power levels (e.g., -9 dbm at 1.3 Gc).

The experiments at this laboratory can be described very briefly. CdSe devices that had been used in experiments with ruby lasers were made available to us by Mr. O. Svelto and Prof. P. D. Coleman of Stanford University. Although strong signals had been observed with ruby lasers at Stanford, we observed no output in our experiments with the He-Ne laser even though the quantum efficiency was essentially 100%; hence R_{eq} must have been less than 0.1 ohm and $\eta^2 R_{eq}$ less than 0.1 ohm.

At the time of the publication it was not clear whether the effect was due to bulk photomixing or to nonlinear interband effects involving transitions between valence and conduction bands. Subsequent analysis has shown the effect to be bulk photomixing[9].

At high light intensities CdSe has such a short decay time that the device can be an efficient photomixer. However, as shown by the experiments at this laboratory, the long decay time of CdSe at low light intensity (e.g., He-Ne laser output of a few milliwatts) leads to a very poor sensitivity. That is, if the decay time is long compared to the microwave period, there is a severe reduction in the microwave output. The problem of building sensitive low-level detectors using this effect reduces to that of finding semiconductors having; (1) high quantum efficiency; and (2) very short decay time at low intensities.

4.5.4 Traveling-Wave Phototubes

In the same experimental apparatus Sylvania microwave phototubes have shown R_{eq} to be $3\text{-}10^5$ ohms and η to be 0.2%. This gives $\eta^2 R_{eq} = 1.2$ ohms.

4.5.5 Conclusions

From the preceding paragraphs it appears that present day photodiodes and TWP's have about the same $\eta^2 R_{eq}$. However, these comparison measurements represent only an initial effort at determining the performance characteristics of various light demodulators. The results obtained are not grossly different from those theoretically predicted by McMurtry and Siegman[10], but at this point it would be unwise to draw firm conclusions from the above data. Such conclusions must await more extensive experimental analysis.

The most important result of these measurements to date is that they led to delineation and clarification of some problem areas for the devices.

In spite of the need for further experimental work one can speculate as to what advances in tubes and diodes one might expect. A photodiode has a theoretical chance to realize unit quantum efficiency ($\eta = 1.0$). If the internal capacitance of the diode is resonated an R_{eq} of many hundreds of ohms might be obtained. Such a diode would have an $\eta^2 R_{eq}$ of perhaps 500 ohms. Of course as a result of the resonant coupling it would be restricted to a narrow bandwidth, and increased bandwidth would be obtained only by sacrificing the relatively high R_{eq}.

With respect to microwave phototubes, the greatest room for improvement lies in the direction of increased quantum efficiency. Tubes having surfaces with $\eta = 6\%$ will be available in the near future. In addition, the R_{eq} of our present 8" TWP can be easily increased to 10^6 by an increase of 2 inches in helix length. Thus $\eta^2 R_{eq}$ would equal 3600 ohms, representing an improvement of more than 30 db.

4.6 Direct Demodulation of Microwave Frequency Modulated Light

In addition to the program on AM demodulators at Sylvania, we have given some attention to methods for demodulating frequency modulated light.

Audio frequency modulated light has been demodulated by optical homodyne techniques[11], and microwave frequency modulated light has been demodulated by using S. Harris' birefringent discriminator[12] and a conventional TWP. The Harris discriminator converts FM into AM by using the natural birefringence of calcite. The device consists of a piece of calcite placed between polarizers.

During this quarter Harris brought a discriminator from Stanford University, and experiments were performed using our modulation-demodulation setup. The light source was a He-Ne laser operating at 6328Å. The laser output was passed through a KDP modulator that was adjusted to impose 3 Gc frequency modulation on the beam. The light was then passed through the discriminator and into a Sylvania SYD-4302A microwave phototube, which produced microwave output at 3 Gc. When the discriminator was removed, microwave output was no longer observed. We believe this to be the first c-w demodulation of microwave frequency modulated light.

4.7 Conclusions

Measurements on TWP's over a wide range of average current, helix voltage and frequency are in good qualitative agreement with the theoretical predictions of Section III. Further experiments and specific calculations must be performed before conclusions can be drawn concerning the quantitative agreement.

Comparison measurements on solid-state photodiodes, devices using bulk effects in CdSe and TWP's have led to clarification of some problem areas for the devices. Firm conclusions concerning the relative merits of the devices must await more extensive experiments.

4.8 Plans for Next Period

The program for the next period is to perform detailed quantitative comparisons between theory and experiment for TWP's, with emphasis on mode width and bandwidth.

SECTION V

CONCLUSIONS

The detailed conclusions presented in the previous sections are summarized in the following paragraphs.

A continuing analysis of light demodulation schemes has reaffirmed the conclusion that the traveling-wave microwave phototube appears to be the most desirable method consistent with the objectives of this applied research program.

The investigation of such devices requires simultaneous efforts in the following areas: (1) theoretical analysis; (2) tube construction; and (3) experimental measurements and comparison theory.

The detailed theoretical analysis presented in Section III has led to a better understanding of the TWP. The rather lengthy conclusions based on R_{eq} calculations are presented in Section 3.7.

Since TWP's are available for our experiments, little work on tube construction needs to be performed in this program.

The experimental measurements on TWP's have shown good qualitative agreement with theoretical predictions.

Comparison measurements on several light demodulators have served to clarify some of the problem areas with each device. However, no firm conclusions should be drawn from the experiments performed to date.

SECTION VI

RECOMMENDATIONS

It is recommended that the program outlined in Section VII be carried out.

SECTION VII

PLANS FOR NEXT PERIOD

The proposed program for the next period is outlined below:

(1) Continue the gun region analysis with emphasis on high average current operation.

(2) Complete the analysis of the G_{eq} calculations and summarize the results.

(3) Continue the multi-velocity beam analysis

(4) Perform detailed quantitative comparisons between theory and experiment for TWP's, with emphasis on mode width and bandwidth.

SECTION VIII

REFERENCES

1. C. F. Quate, "Shot Noise from Thermionic Cathodes," in Noise in Electron Devices, ed. by L. D. Smullin and H. A. Haus, Wiley, 1959.

2. A. E. Siegman, "Microwave Noise Fluctuations in the Potential-Minimum Region of an Electron Beam," Technical Report No. 401-1, Stanford Electronic Laboratories, Stanford, California, April 1957.

3. A. Ashkin, W. H. Louisell, and C. F. Quate, "Fast Wave Couplers for Longitudinal Beam Parametric Amplifiers," Journal of Electronics and Control, Vol. 7, July 1959, p. 5.

4. J. R. Pierce, Traveling-wave Tubes, New York. D. Van Nostrand, 1950.

5. R. P. Riesz, "High Speed Semiconductor Photodiodes," Rev. Sci. Instr., Vol. 33, September 1962, pp. 994-998.

6. H. Inaba and A. E. Siegman, "Microwave Photomixing of Optical Maser Outputs with a PIN-Junction Photodiode," Proc. of IRE, Vol. 50 August 1962, pp. 1823-24.

7. G. Lucovsky, M. E. Lasser and R. B. Emmons, "Coherent Light Detection in Solid-State Photodiodes," Proc. IEEE, Vol. 51, January 1963, pp. 155-172.

8. M. DiDomenico, Jr., et al, "Optical Frequency Mixing in Bulk Semiconductors," Applied Physics Letters, Vol. 1, December 1962 pp. 77-79.

9. O. Svelto, M. DiDomenico, Jr., R. H. Pantell, Private Communications.

10. B. J. McMurtry and A. E. Siegman, "Broadband Demodulators for Microwave-Modulated Light," Proceedings of the Symposium on Optical Processing of Information, Washington, D. C., October 1962.

11. P. Rabinowitz et al, "Homodyne Detection of Phase-Modulated Light," Proc. IRE, Vol. 50, November 1962, p. 2365.

12. S. E. Harris "Conversion of FM Light to AM Light Using Birefringent Crystals," Applied Physics Letters, Vol. 2, February 1, 1963, pp. 47-49.

DISTRIBUTION LIST FOR INTERIM
ENGINEERING REPORTS

CONTRACT AF 33(657)-8995

COPIES	ORAGANIZATION
10	ASTIA (TIPDR) Arlington Hall Station Arlington 12, Virginia
4	Advisory Group on Electron Devices 346 Broadway, 8th floor New York 13, New York
1	U. S. Army Signal Research and Development Laboratories (SIGRA/SL-PRT) F rt Monmouth, New Jersey
1	Chief, BuShips Attention: Code 681A1D Navy Department Washington 25, D. C.
2	Aeronautical Systems Division (ASRNET-3) Wright-Patterson Air Force Base Ohio
1	Aeronautical Systems Division (ASRNRS-2) Wright-Patterson Air Force Base Ohio
1	Watkins-Johnson Company Stanford Industrial Park Attention: Dr. Stanley Sobottka 3333 Hillview Avenue Palo Alto, California
1	Radio Corporation of America Electron Tube Division Attention: Dr. F. Sterzer Princeton, New Jersey
1	Evans Signal Laboratory Attention: Mr. S. Schneider Fort Monmouth, New Jersey
1	Westinghouse Electric Corporation Attention: Mr. Gerald I. Klein Air Arm Division 32 North Main Street Dayton 2, Ohio

COPIES	ORGANIZATION
1	Hughes Research Laboratories Attention: Dr. M. R. Currie 3011 Malibu Canyon Road Malibu, California
1	Raytheon Company Research Division Attention: Dr. P. A. Lindsay Waltham 54, Massachusetts
1	General Electric Company Power Tube Department Attention: Dr. F. B. Fank Palo Alto, California
1	The Bendix Corporation Research Laboratories Division Attention: Mr. G. W. Goodrich Southfield, Michigan
1	ITT Federal Laboratories Components and Instrumentation Laboratory Attention: Dr. D. K. Coles Fort Wayne, Indiana
1	Technical Research Group, Inc. Attention: Dr. Richard T. Daly 2 Aerial Way Syosset, New York
1	Sperry Gyroscope Company Division of Sperry Rand Corp. Attention: Dr. George White Great Neck, New York
1	Microwave Electronics Corp. Attention: Dr. Robert W. DeGrass 4061 Transport Street Palo Alto, California
1	Quantum Electronics Laboratories Quantatron, Incorporated Attention: R. A. Gudmundsen 2109 West Wright Street Santa Ana, California

DISTRIBUTION LIST FOR
INTERIM ENGINEERING REPORTS (cont.)

COPIES	ORGANIZATION
1	Philco Corporation Western Development Laboratories Library 3825 Fabian Way Palo Alto, California
1	National Engineering Science Company Attention: Dr. Gunnar Bergman 711 S. Fair Oaks Avenue Pasadena, California
1	AFCRL (CRRSQ) Attention: P. Schweitzer L. G. Hanscom Field Bedford, Massachusetts
1	University of California Electronics Engineering Department Attention: Ralph Kalibjian Livermore, California
1	RADC (RAALD) Attention: Document Library Griffiss Air Force Base New York
1	Redstone Scientific Information Center U. S. Army Missile Command Attention: Chief, Document Section Redstone Arsenal, Alabama
1	The Machlett Laboratories, Inc. Attention: S. T. Yanagisawa Product Line Manager Photosensitive & Display Division Springdale, Stamford, Connecticut
1	U.S. Department of Commerce National Bureau of Standards Boulder Laboratories Boulder, Colorado